Crystalline Morphology and Polymorphic Phase Transitions in Electrospun Nylon-6 Nanofibers

Yi Liu,[†] Li Cui,[‡] Fangxiao Guan,[‡] Yi Gao,[†] Nyle E. Hedin,[†] Lei Zhu,*[,‡] and Hao Fong*[,†]

Department of Chemistry, South Dakota School of Mines and Technology, Rapid City, South Dakota 57701, and Polymer Program, Institute of Materials Science and Department of Chemical, Materials and Biomolecular Engineering, University of Connecticut, Storrs, Connecticut 06269

Received January 5, 2007; Revised Manuscript Received June 11, 2007

ABSTRACT: Uniform nylon-6 nanofibers with diameters around 200 nm were prepared by electrospinning. Polymorphic phase transitions and crystal orientation of nylon-6 in unconfined (i.e., as-electrospun) and a high T_g (340 °C) polyimide confined nanofibers were studied. Similar to melt-spun nylon-6 fibers, electrospun nylon-6 nanofibers also exhibited predominant, metastable γ-crystalline form, and the γ-crystal (chain) axes preferentially oriented parallel to the fiber axis. Upon annealing above 150 °C, γ-form crystals gradually melted and recrystallized into thermodynamically stable α-form crystals, which ultimately melted at 220 °C. Release of surface tension accompanied this melt−recrystallization process, as revealed by differential scanning calorimetry. For confined nanofibers, both the melt−recrystallization and surface tension release processes were substantially depressed; γ-form crystals did not melt and recrystallize into α-form crystals until 210 °C, only 10 °C below the T_m at 220 °C. After complete melting of nanoconfined crystals at 240 °C and recrystallization at 100 °C, only α-form crystals oriented perpendicular to the nanofiber axis were obtained. In the polyimide-confined nanofibers, the Brill transition (from the monoclinic α-form to a high-temperature monoclinic form) was observed at 180−190 °C, which was at least 20 °C higher than that in unconfined nylon-6 at ∼160 °C. This, again, was attributed to the confinement effect.

Introduction

Nylon-6, also known as polycaprolactam and polyamide-6, possesses excellent physical and mechanical properties and is one of the most widely used synthetic polymers for fibers. Nylon-6 fibers exhibit both crystalline and amorphous phases, with the amorphous phase consisting of isotropic and anisotropic components.[1,2] It is believed that the detailed structures and morphologies of the crystalline phases are important to the nylon-6 properties.[3−5] Nylon-6 has two common crystalline forms, α- and γ-forms, and these two crystalline forms coexist in nylon-6 fibers in various percentages depending on processing conditions.[6−8] It is generally recognized that the α-form crystal is composed of extended nylon-6 chains and the γ-form crystal is composed of pleated chains. Hydrogen bonding is primarily intrasheet in the α-crystalline form and intersheet in the γ-crystalline form.[9] Since the hydrogen-bonding direction in the γ-form is about 60° from the original hydrogen-bonding direction in the α-form, a hexagonal or pseudohexagonal packing is resulted in the γ-form. The different structures of α- and γ-crystalline forms impart different physical and mechanical properties. For example, the Young's modulus of the α-form crystal is higher than that of the γ-form crystal. Although the α-form is more thermodynamically favorable/stable and is the preferred structure in solution-cast and annealed nylon-6 samples, the γ-crystalline form has been noted to predominate in melt-spun nylon-6 fibers and nylon-6/clay nanocomposites.[10−15] It is generally believed that rapid crystallization favors γ-form and slow crystallization favors the α-form.[16]

Electrospinning is a technique that utilizes electric force alone to drive the spinning process and to produce polymer fibers from solutions (or melts).[17−21] Unlike conventional spinning techniques (e.g., solution- and melt-spinning), which are capable of producing fibers with diameters in the micrometer range (ca. 5−15 μm), electrospinning is capable of producing fibers with diameters in the nanometer range (ca. 50−500 nm). Electrospun nanofibers possess many unique properties including small diameters and large specific surface areas, a high degree of structural perfection, and superior mechanical properties. Unlike carbon nanotubes that are produced by synthetic, bottom-up methods, electrospun nanofibers are produced through a top-down nanomanufacturing process, which results in low-cost electrospun nanofibers that are also relatively easy to align, assemble, and process into devices.[22] Therefore, electrospinning and the resulting nanofibers are of great scientific, military, and commercial interests and have been widely investigated in the past decade.[23−30]

In electrospinning, a spin dope (e.g., a polymer solution with a viscosity similar to that of honey) is placed in a container (e.g., a regular glass pipet), and a high dc voltage, usually in the range from 5 to 40 kV, is applied to the solution through an electrode (e.g., a copper wire). An electrically grounded collector is placed at a distance (known as gap distance) from the spinneret ranging from centimeters to 1 m. When the electrostatic field reaches a critical value and the electric force overcomes the surface tension and the viscoelastic force, a jet is ejected and travels straightly for a certain distance (known as the jet length). The jet then starts to bend, forming spiral and expanding loops. This phenomenon is termed "bending instability"[25,31,32] or "whipping instability".[33] Typically, the bending instability results in an elongated jet of more than 10 000× draw ratio in a very short time period (50 ms or less). Thus, the draw rate during bending instability is extremely high

* Corresponding authors. Lei Zhu: Tel (860) 486-8708, Fax (860) 486-4745, e-mail lei.zhu@uconn.edu. Hao Fong: Tel (605) 394-1229, Fax (605) 394-1232, e-mail Hao.Fong@sdsmt.edu.
[†] South Dakota School of Mines and Technology.
[‡] University of Connecticut.

10.1021/ma070039p CCC: $37.00
Published on Web 07/27/2007

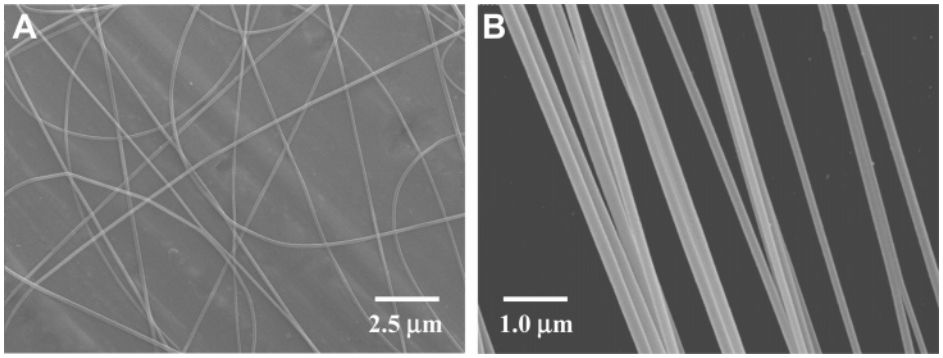

Figure 1. Representative SEM images of electrospun nylon-6 nanofibers: (A) collected on aluminum foil covered on the roller; (B) collected with the U-shaped metal device and then transferred onto a conducting tape.

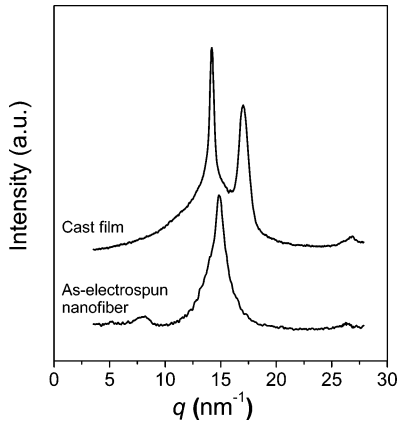

Figure 2. One-dimensional (1D) WAXD profiles of as-electrospun nanofiber and cast film of nylon-6.

(up to 1 000 000 s^{-1}). Such large draw ratio and draw rate are capable of aligning the macromolecular chains along the nanofiber axis. The solvent removal in electrospinning occurs by evaporation, whereas the solvent removal in conventional wet-spinning uses a coagulation bath.[34] Note that although all commercial aliphatic nylon fibers are melt-spun, wet-spinning appears to be a viable comparison because solvents are used in both processing methods. In conventional wet-spinning, microvoids and other structural defects often form in the as-spun fibers during the rapid solvent extraction in the coagulation bath, whereas they are significantly suppressed in electrospun nanofibers. The fast elongation/drawing of an electrospinning jet often occurs in the solution and/or gel state, and thus highly oriented macromolecular chains should exist in the jet formation stage. However, these oriented chains could relax after the bending instability, especially when the collected electrospun nanofibers still contain a small amount of solvent. Like conventional wet-spun fibers, electrospun nanofibers may also be poststretched, and better macromolecular orientation and mechanical properties could be achieved.[35]

Although electrospinning has been actively researched for years and many polymers have been successfully electrospun into nanofibers, only a limited number of papers have appeared in the literature reporting on the macromolecular orientation and crystalline structures in polymer nanofibers.[36−38] Nylon-6 nanofibers with diameters ranging from tens to hundreds of nanometers, for example, have been successfully electrospun from hexafluoroisopropanol solutions[24,36] and have been investigated as reinforcement materials in nanocomposites.[39,40] Little is known about the crystalline structures (e.g., α- or γ-form) of nylon-6 and their transitions in electrospun nanofibers. Murase and co-workers found that the macromolecular orientation and crystalline structure of nylon-6 in conventional fibers depended markedly on process conditions such as the take-up speed,[41] with the γ-form predominant when the take-up speed was 6 km/min and below and the α-form predominant when the take-up speed was greater than 9 km/min.

The objective of this study is to understand the macromolecular orientation, crystalline structure, and polymorphic phase transition of electrospun nylon-6 nanofibers under both unconfined and confined conditions. Nylon-6 nanofibers with a diameter of ∼200 nm were electrospun from hexafluoroisopropanol solutions and collected either as a loosely oriented fabric or as a highly aligned bundle. The morphology of nylon-6 nanofibers was examined by scanning electron microscopy (SEM), and macromolecular orientation and polymorphic phase transitions of nylon-6 in the nanofibers were investigated using polarized Fourier transform infrared (FTIR), differential scanning calorimetry (DSC), and wide-angle X-ray diffraction (WAXD). To study polymorphic phase transitions of nylon-6 in nanoconfined environments, the as-electrospun (unconfined) nanofibers were coated (confined) with an organosoluble polyimide (PI) having a high glass transition temperature (T_g ∼ 340 °C). Experimental results indicated that (1) the γ-form was predominant in the as-electrospun nylon-6 nanofibers, (2) the metastable γ-form transformed into the thermodynamically stable α-form via a melt−recrystallization process during heating or annealing at elevated temperatures, (3) confinement of the nanofibers with PI caused the melt−recrystallization to take place at a much higher temperature, close to the actual melting temperature (T_m), (4) nylon-6 chains were oriented parallel to the fiber direction in the unconfined (as-electrospun) nanofibers, while the chains were oriented perpendicular to the fiber direction in the PI-confined and melt−recrystallized nanofibers, and (5) the Brill transition in nanoconfined nylon-6 fibers was observed to be at least 20 °C higher (at ∼180 °C) than that for unconfined nylon-6 (at 160 °C).

Experimental Section

Sample Preparation. The general electrospinning process and the mechanism of electrospinning should refer to previous reports.[25,31] In this work, a solution of 8 wt % nylon-6 (Aldrich catalog number: 181110; weight-average molecular weight M_w = 10 000 g/mol) in 1,1,1,3,3,3-hexafluoro-2-propanol (Aldrich) was prepared at room temperature, and a specially designed spinneret was used for conducting electrospinning. The spinneret consisted of a high-density polypropylene tube (an inner diameter of ∼1.0 in.) and a stainless steel hemispherical head which had an orifice of 0.4 mm diameter at the center. The electrospinning setup also consisted of a high-voltage power supply (Gamma High Voltage Research, Ormond Beach, FL) and a home-built roller (with a diameter of ∼10 in.). During electrospinning, a positive high voltage of 25 kV was applied through a metal rod to the solution held inside the spinneret. Nylon-6 nanofibers were collected on the roller covered

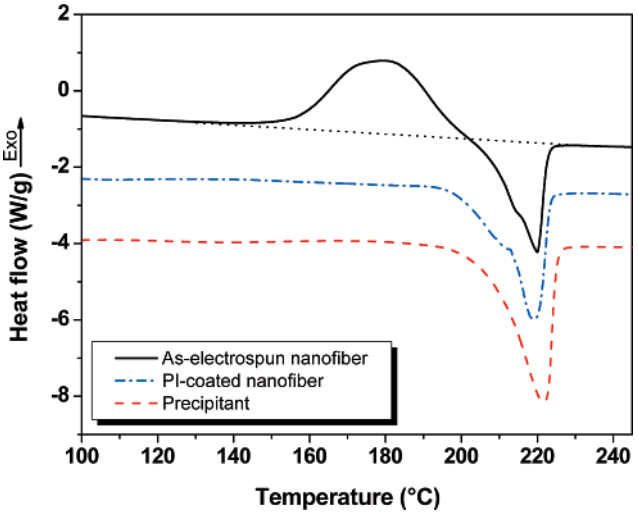

Figure 3. DSC traces of as-electrospun nylon-6 nanofibers (solid line), nylon-6 solution precipitant (dashed line), and polyimide-coated nylon-6 nanofibers (dash−dot line) at a heating rate of 10 °C min^{-1}.

with electrically grounded aluminum foil. The rotational speed of the roller during electrospinning was 100 rpm. In this manner electrospinning was extremely stable, with the electrospinning jet running continuously without breaking for several hours. The obtained fabric on the aluminum foil was thus hypothetically a single nanofiber loosely aligned along the rolling direction. A heating lamp was employed to dry the collected nylon-6 nanofibers during the electrospinning process. The collected nylon-6 nanofibers were subsequently dried in a vacuum oven at room temperature for 12 h. To obtain a highly aligned nylon-6 nanofiber bundle, a U-shaped metal device (the distance between the two legs was ∼25 mm) was used. By manually moving the electrically grounded device back and forth 2 to 3 times between the spinneret and the roller during electrospinning, tens to hundreds of highly aligned nylon-6 nanofibers could be collected between the metal legs. This U-shaped device functioned like a traverse guide in a conventional wind-up, and a skein of aligned nanofibers could be formed on the device. These nanofibers were then transferred to a slightly smaller U-shaped metal device for further analysis, and the process was repeated for ∼50 times to collect an aligned nylon-6 nanofiber bundle.

An organosoluble polyimide (6FDA-PFMB) of 2,2-bis(3,4-dicarboxyphenyl)hexafluoropropane dianhydride (6FDA) and 2,2-trifluoromethyl-4,4-diaminobiphenyl (PFMB) was used to confine the nylon-6 nanofibers. The as-electrospun nanofibers were repeatedly dipped into a 1 wt % 6FDA-PFMB/acetone solution, followed by drying in a vacuum oven at room temperature for 24 h. Because the T_g of 6FDA-PFMB is around 340 °C,[42] which is much higher than the nylon-6 T_m of ∼220 °C, the phase transitions of nylon-6 were effectively confined within the nanofibers.

Sample Characterization. The morphology of unconfined (as-electrospun) nylon-6 nanofibers was examined using a JEOL-840A SEM. Polarized FTIR spectra of nylon-6 in electrospun nanofibers were obtained using a Bruker Tensor-27 FTIR spectrometer equipped with a liquid nitrogen-cooled mercury−cadmium telluride (MCT) detector. Samples were prepared by pressing the aligned nylon-6 nanofibers with potassium bromide, and the FTIR spectra were acquired by scanning the samples (64 scans) from 600 to 4000 cm^{-1} with a resolution of 4 cm^{-1}. DSC experiments were carried out on a TA Q-100 DSC instrument. Less than 1.0 mg of sample was used for the DSC study to avoid possible thermal lag. The scanning rate was 10 °C/min for both heating and cooling runs.

WAXD experiments were carried out both in house and at national synchrotron X-ray facility in Brookhaven National Laboratory (BNL). For the in-house WAXD experiments, a Bruker X-ray tube operating at 1.6 kW with the Cr Kα radiation (wavelength λ = 0.229 nm) was used. Two-dimensional (2D) WAXD data were recorded at room temperature, using a Bruker AXS area detector with a general area detector diffraction system (GADDS). Synchrotron 2D WAXD experiments were performed at X27C beamline in the National Synchrotron Light Source (NSLS) at BNL. The wavelength of the X-ray beam was 0.137 nm. The beam center was calibrated using silver behenate with the first reflection peak at the scattering vector $q = (4\pi \sin\theta)/\lambda = 1.076$ nm^{-1}, where θ is the half scattering angle and λ is the wavelength. Fuji imaging plates were used as X-ray detectors, and a typical data acquisition time was 1 min. Digital WAXD images were obtained using a Fuji BAS-2500 scanner. Temperature-dependent X-ray experiments were performed using an Instec HCS410 hot stage, equipped with a liquid nitrogen cooling accessory. In both in-house and synchrotron X-ray experiments, one-dimensional (1D) results were obtained by integration of the corresponding 2D WAXD patterns using Polar 2.6.9 software (Stony Brook Technology and Applied Research, Inc.). Azimuthal profiles were obtained from 2D WAXD patterns with the zero angle on the equator and counterclockwise scanning.

Results and Discussion

Macroscopic Morphology of Electrospun Nylon-6 Nanofibers. Figure 1 shows representative SEM images of electrospun nylon-6 nanofibers. The diameter of nanofibers was ∼200 nm, and the nanofibers were smooth (without microscope identifiable beads and/or beaded nanofibers) and uniform (with only small variations in diameter). The nanofibers collected with the home-built roller were loosely oriented along the rolling direction (see Figure 1A), whereas the nanofibers collected with the U-shaped metal device were highly aligned (see Figure 1B). Note that by using only the roller (or similar devices), it is unlikely to achieve a high degree of nanofiber alignment since the formation of electrospun nanofibers results from "bending instability",[25,31,32] which makes the traveling path/trajectory of electrospinning jet/fiber completely random. Although the unidirectional rotation can introduce a certain degree of nanofiber alignment, the alignment is far from uniform. To achieve a high degree of nanofiber alignment with a small amount of sample, the U-shaped metal collecting device was adopted. If the required sample amount is large, a roller could be used, but the collected nanofibers might have to undergo a post-electrospinning stretching process to be further aligned.

The crystalline structures of nylon-6 in the as-electrospun nanofibers were characterized by WAXD, and the result was compared with that acquired from a cast film (prepared from the same solution used for electrospinning). As evident in Figure 2, the as-electrospun nylon-6 nanofibers displayed (020) and (200) diffraction peaks at 7.95 and 14.9 nm^{-1} (d-spacing = 0.790 and 0.421 nm, respectively), characteristic of the γ-crystalline structure. The nylon-6 in the cast film, on the other hand, showed two diffraction peaks, (200) and mixed (002)/(202), at 14.2 and 17.0 nm^{-1} (d-spacing = 0.442 and 0.369 nm, respectively), which are characteristic of the α-crystalline structure. Similar to conventional spinning techniques,[15] WAXD results indicated that electrospinning could also result in the formation of γ-crystalline structure for nylon-6. Since the formation of γ-crystalline structures requires a rapid crystallization rate, this suggests that nylon-6 crystallization was rapid during electrospinning. The crystallinity of as-electrospun nylon-6 nanofibers was less and the reflection peak was broader than for the solution-cast film, suggesting that the sizes of nylon-6 crystallites were smaller in the electrospun nanofibers. Using Scherrer analysis,[43] the average crystallite size for the $(200)_\gamma$ reflection of the as-electrospun nanofibers was ∼5.1 nm, whereas the average crystallite size for the $(200)_\alpha$ reflection in the solution-cast nylon-6 was ∼13.8 nm.

Melting Behaviors of Unconfined and Confined Nylon-6 Nanofibers. The changes in crystallinity of both unconfined

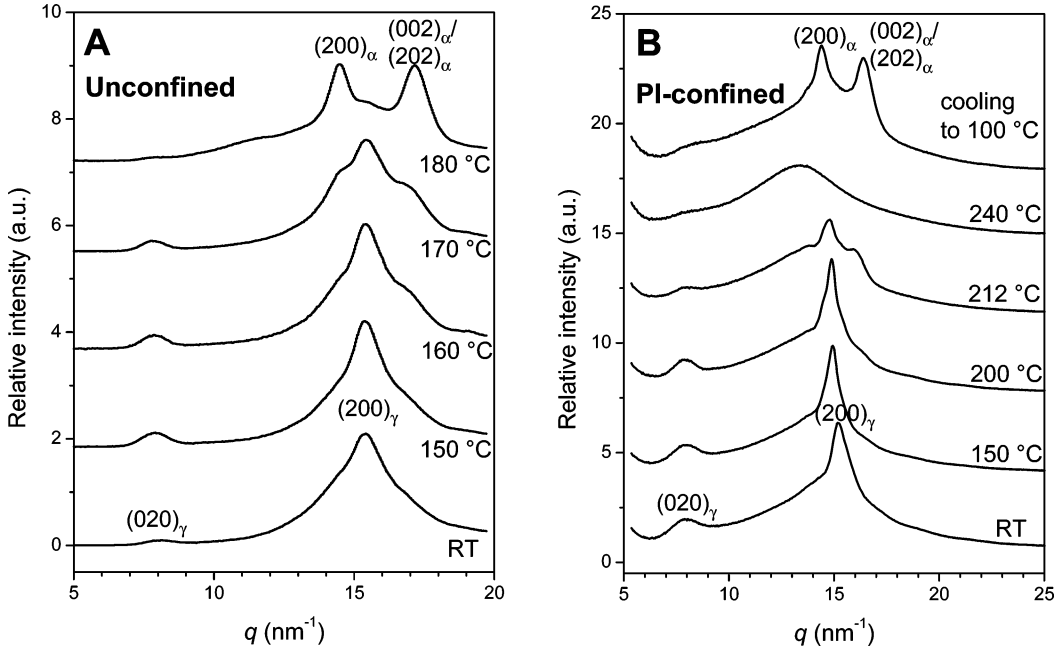

Figure 4. One-dimensional (1D) WAXD profiles for (A) unconfined (as-electrospun) and (B) confined (polyimide-coated) nylon-6 nanofibers at different temperatures. For unconfined nylon-6 nanofibers, the sample was annealed at each temperature for 24 h. For polyimide-confined nylon-6 nanofibers, the sample was held at each temperature for 15 min. The WAXD profiles in (A) were obtained using the in-house X-ray instrument, whereas the profiles in (B) were obtained using synchrotron X-ray facility. Different peak widths in (A) and (B) originate from different X-ray instruments.

and confined nylon-6 nanofibers upon thermal treatment were investigated by DSC at a heating rate of 10 °C min^{-1}, and the results are shown in Figure 3. For comparison, the solution precipitant of nylon-6 was also examined by DSC at the same heating rate. The solution precipitant was prepared using the same nylon-6 solution for electrospinning, and the precipitation was conducted in diethyl ether with vigorous stirring, followed by drying in a vacuum oven to a constant weight. The precipitant showed a single melting peak at 222 °C with a crystallinity of 30 wt %. The heat of fusion for perfect α-form crystals is 241 J/g.[44] For unconfined nylon-6 nanofibers, an exothermic peak occurred at ~180 °C, while no such peak was seen for the PI-confined nylon-6 nanofibers. The crystallinities of the unconfined and confined nylon-6 nanofibers were 22 wt % (the endothermic peak below the dotted line) and 27 wt %, when the heat of fusion is taken as 239 J/g for perfect γ-form crystals.[44] There may be three reasons accounting for the exothermic peak for unconfined nylon-6 nanofibers: (1) direct (or cold) crystallization of nylon-6 from the amorphous phase, (2) transformation from the less thermodynamically stable γ-form to the more thermodynamically stable α-form via a melt recrystallization process, and (3) release of surface tension generated during the fast drying process of the nanofibers in electrospinning. The disappearance of the exothermic peak for PI-confined nanofibers ruled out the first possibility. Note that the integrated area of this exothermic peak is 100% greater than that of the melting peak at 220 °C. This indicated that surface tension release was a significant contribution to the exothermic peak, similar to the phenomenon observed for PS microbeads.[45]

To better understand the melting behaviors of unconfined and confined nylon-6 nanofibers, 1D WAXD studies were performed at various temperatures. Figure 4A shows room temperature WAXD results of nylon-6 nanofiber bundles after annealing at 150, 160, 170, and 180 °C for 24 h. Compared with the WAXD profile at room temperature, the overall γ- and α-crystallinity slightly increased with increasing temperature up to 150 °C. When the annealing temperature reached 170 °C, the α-form (200) and mixed (002)/(202) reflections became more pronounced. After annealing at 180 °C for 24 h, the γ-form crystallinity nearly disappeared and α-form crystals became predominant.

For *n*-nylons, the α-phase is more stable than the γ-phase for $n \leq 5$, whereas the γ-phase is believed to be more stable for $n \geq 8$.[16] For nylon-6, however, the free energies of the α- and γ-forms are fairly close to each other because (1) both the α- and γ-forms may not interconvert before melting under common DSC heating conditions, (2) the γ-form can transform into the α-form upon use of certain solvents, and (3) the α-form can convert into the γ-form using the iodination process.[16] More interestingly, depending on the relative metastability of the α- and γ-forms crystallized under different experimental conditions, the α-form can transform into the pseudohexagonal form (which could be considered as a high-temperature version of the γ-form) via a crystal-to-crystal transition, or the γ-form may transform into the α-form via melt−recrystallization during a very slow heating process. These two transformations are illustrated using the Gibbs free energy diagrams in Figure 5A,B. In both diagrams, the α-form is always more stable than the γ-form or the pseudohexagonal form (γ*) at low temperatures. Figure 5A shows the so-called reversible Brill transition, where the free energy curve of the γ- or γ*-phase intercepts those for both the α-form and the equilibrium melt. As a result, upon heating the α-form transforms, through a direct crystal-to-crystal transition, into the γ- or γ*-form for most nylons or a high-temperature monoclinic form for nylon-6.[1,16] The origin of the Brill transition was believed to arise from the twist in the methylene unit adjacent to the amide groups, as determined by FTIR spectroscopy and X-ray diffraction with molecular modeling.[46]

When the free energy curve for the γ-form only intercepts the equilibrium melt but not that of the α-form, a situation is depicted in Figure 5B. During a relatively fast heating process, the γ-form crystals directly melt without transforming into the α-form crystals. During a very slow heating, however, the

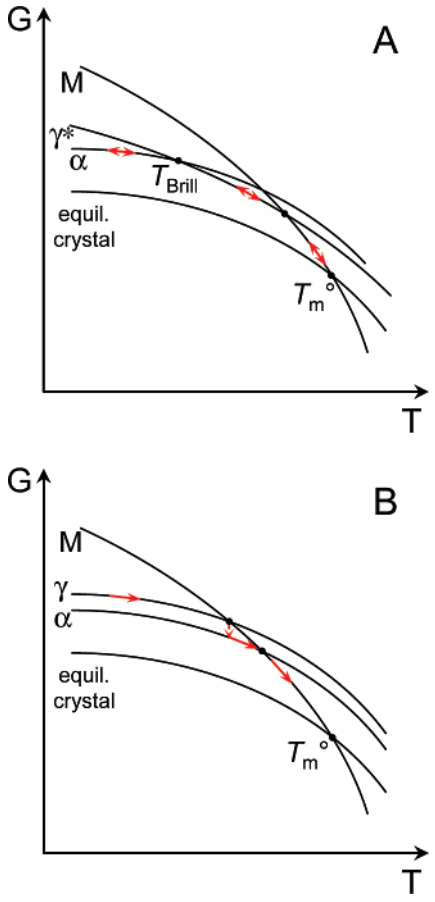

Figure 5. Gibbs free energy diagrams for (A) a Brill transition, where the α-form transforms into the pseudohexagonal form (γ*) at T_{Brill}, and (B) a melt−recrystallization process, where the γ-form transforms into the α-form upon a heating process (indicated by arrows). Note that the equilibrium crystal transforms into the melt (M) at the equilibrium melting temperature ($T_m°$).

γ-form melts and then recrystallizes into the α-form, followed by melting at a higher temperature (see arrows in Figure 5B). Obviously, results in Figure 4A clearly indicate that the above-observed γ-to-α transition upon slow heating is different from the Brill transition and should be explained by a melt−recrystallization process. When the sample was annealed at 180 °C or above, the nanofibers eventually fused together as observed by optical microscopy (data not shown). This further supports the existence of a melt−recrystallization process during slow heating for unconfined nylon-6 nanofibers.

Intriguingly, the melt−recrystallization process was substantially depressed after the nanofibers were coated by the PI, as shown in Figure 4B. For example, γ-form crystals started to melt and recrystallized into α-form crystals above 210 °C (only 10 °C below the T_m at 220 °C) because the α-form (200) and (002)/(202) reflections appeared and the γ-form (020) reflection became weaker. Additionally, because of the PI nanoconfinement effect, the release of surface tension (the broad exothermic peak) was also suppressed, as demonstrated in the DSC trace in Figure 3 for PI-confined nylon-6 nanofibers. At 240 °C, the nylon-6 crystals completely melted. After slow cooling back to 100 °C, only α-form crystals were observed in the PI-confined nanofibers.

Crystal Orientation in Nylon-6 Nanofibers. FTIR equipped with a polarizer was employed to examine the molecular orientation in the electrospun nylon-6 nanofibers. The sample used in this study was collected with the U-shaped metal device, and the nanofibers form highly aligned bundles. It was found

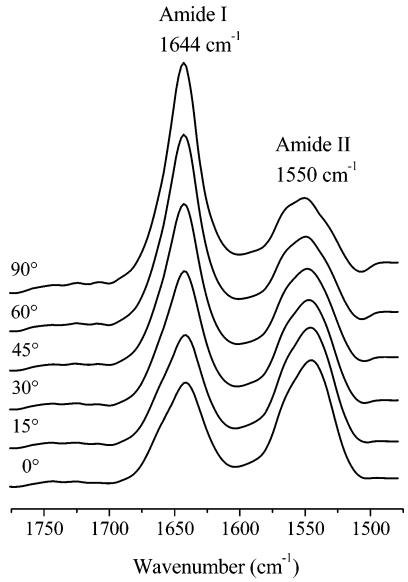

Figure 6. Polarized FTIR spectra of the aligned nylon-6 nanofibers. From top to bottom, the spectra were collected at the incident angles of 0°, 15°, 30°, 45°, 60°, and 90°. The zero angle was defined as the FTIR beam parallel to the nanofiber axes.

that the characteristic amide I ($\nu_{C=O}$ at 1644 cm^{-1}) and amide II (δ_{N-H} at 1550 cm^{-1}, consistent with a trans conformation) absorptions of nylon-6 were sensitive to the incident beam polarization angle (the angle between the polarized infrared beam and the axes of the aligned nanofibers). Polarized FTIR spectra of the aligned nylon-6 nanofibers as a function of the incident angle are shown in Figure 6. From bottom to top, six spectra were collected at incident angles of 0° (parallel), 15°, 30°, 45°, 60°, and 90° (perpendicular), respectively. With increasing the incident angle from 0° to 90°, the intensity of the amide I band gradually increased, while the intensity of the amide II absorption band decreased. A qualitative explanation of the dependence of the amide I band intensity with respect to the incident angle may be as follows. At an incident angle of 0°, the axes of the aligned fibers are parallel to the direction of the electric field of the incoming IR beam. Assuming the macromolecular chains of nylon-6 are aligned along the nanofiber axis, one would expect the carbonyl groups to be perpendicular to the fiber axis (90° to the fiber axis). Therefore, absorption of the incoming IR beam by the C═O bonds is minimal at 0°. When the fiber axis is perpendicular to the incident beam (90°), amide I absorption reaches a maximum as a result of the resonance between the carbonyl stretching and the electric field of the incoming IR beam. On the other hand, N−H bending direction is almost perpendicular to the molecular chain direction. When the molecular chains are parallel to the fiber direction, the amide II absorption is the maximum at an incident angle of 0°, since the N−H bending direction is almost parallel to the electrical field of the polarized IR beam. As the incident angle is increased to 90°, the N−H bending direction becomes perpendicular to the electrical field of the polarized IR beam, and the amide II absorption is the weakest. Taking into account both trends in the amide I and amide II absorption together, the gradual increase of the amide I absorption and gradual decrease of the amide II absorption with the incident angle changing from parallel to perpendicular indicated that nylon-6 macromolecular chains were aligned along the nanofiber axis. Note that both crystalline and amorphous nylon-6 contributed to the amide I and II absorption bands, and the crystallinity of the as-electrospun nanofibers was only 22 wt %. The substantial absorption change at different incident

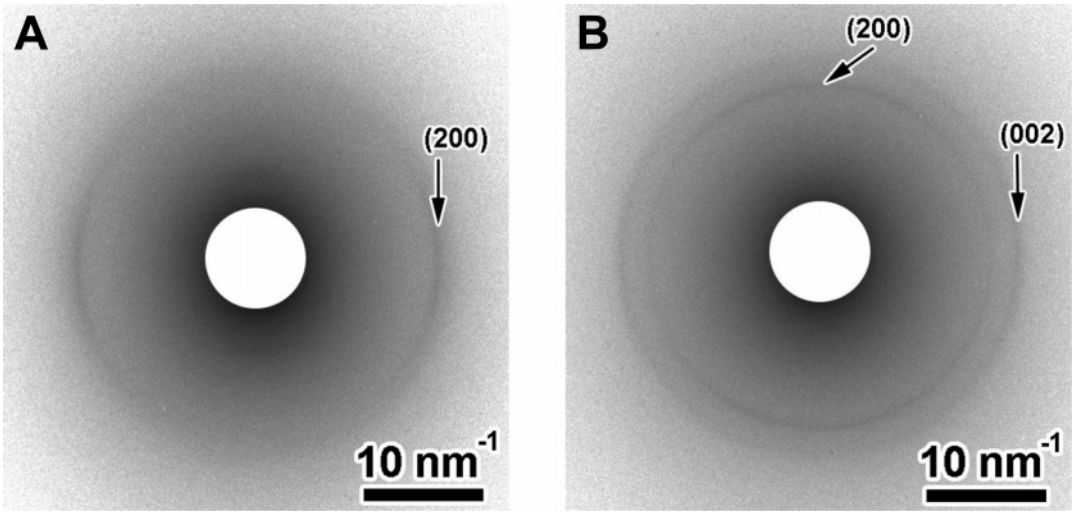

Figure 7. Two-dimensional (2D) WAXD patterns for (A) as-electrospun and (B) melt-recrystallized nylon-6 nanofibers coated with polyimide. The fiber direction is vertical.

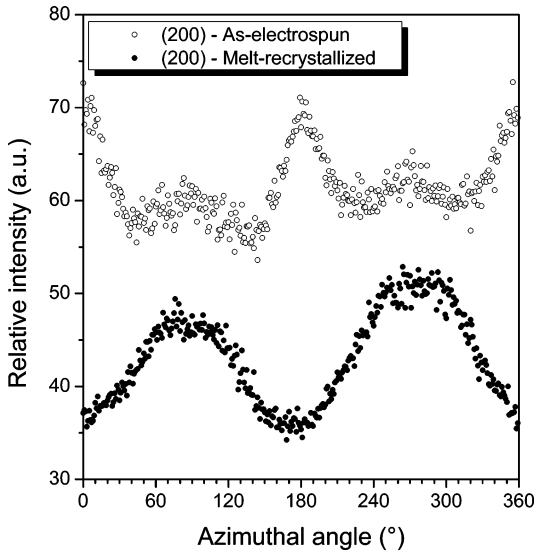

Figure 8. Azimuthal-scan profiles for the $(200)_\alpha$ and $(200)_\gamma$ reflections for as-electrospun and melt-recrystallized nylon-6 nanofibers coated with polyimide. The profiles were offset for clarity.

angles suggested that a significant amount of amorphous nylon-6 chain might also adopt more or less parallel orientation along fiber axes due to rapid solvent evaporation followed by vitrification (nylon-6 $T_g \sim 50$ °C) in electrospinning.

The crystal (or chain) orientation in nylon-6 nanofibers was further investigated by 2D WAXD experiments, and results are shown in Figure 7. Figure 7A shows the 2D WAXD pattern for the as-electrospun nanofibers. The γ-form $(200)_\gamma$ reflection was observed on the equator, and the azimuthal scan result of the $(200)_\gamma$ reflection is shown in Figure 8 (open circles). Two maxima are observed at 0° and 180°, indicating that the *a*-axes of the γ-form crystals were perpendicular to the fiber direction. This confirms our previous conclusion from polarized FTIR that the chain axis (the crystal *b*-axis) is parallel to the fiber direction. After the complete melting of γ-form crystals in the PI-coated nanofibers by heating them to 250 °C, the sample was isothermally crystallized at 100 °C and α-form crystals were obtained. The 2D WAXD pattern for the α-form crystals is depicted in Figure 7B. The azimuthal scan result of the $(200)_\alpha$ reflection is shown in Figure 8 (solid circles). Two broad maxima were seen around 90° and 270°, suggesting that the

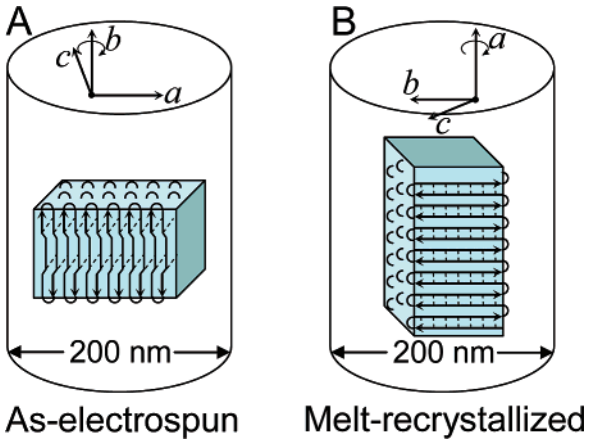

Figure 9. Schematic representations of the crystal orientation in (A) as-electrospun and (B) melt-recrystallized nylon-6 nanofibers coated with polyimide. Dashed lines represent hydrogen bonding.

a-axes of α-crystals were parallel to the fiber direction. In other words, the chain axis (the crystal *b*-axis) is perpendicular to the PI-confined nanofiber direction.

On the basis of the above results, molecular models of both as-electrospun and melt-recrystallized nanofibers confined by PI are shown in Figure 9. In the electrospinning process, nylon-6 chains experienced substantial stretch and the molecular chains eventually oriented along the nanofiber direction. With this chain orientation, the γ-form lamellar crystals were oriented perpendicular to the fiber direction, and the lateral crystallite sizes could be limited by the nanofiber diameter of ~200 nm or crystal impingement, depending upon the nucleation density. This is consistent with the WAXD observation in Figure 2 that the $(200)_\gamma$ reflection is relatively broad. However, after melt−recrystallization in the PI-confined nanofibers, crystal growth along the fiber direction was favored. When the fast growth direction was along the *a*-axes of α-form crystals, the crystalline lamellae would orient parallel to the fiber axis as shown in Figure 9B.

To examine nanoconfinement effect on nylon-6 Brill transition, the PI-confined electrospun nanofibers were subject to a heating and cooling cycle, and the corresponding 1D WAXD results are shown in Figure 10. Upon heating, the $(200)_\alpha$ and $(002)_\alpha/(202)_\alpha$ reflections gradually shifted toward each other above 100 °C. However, both reflections almost stopped shifting

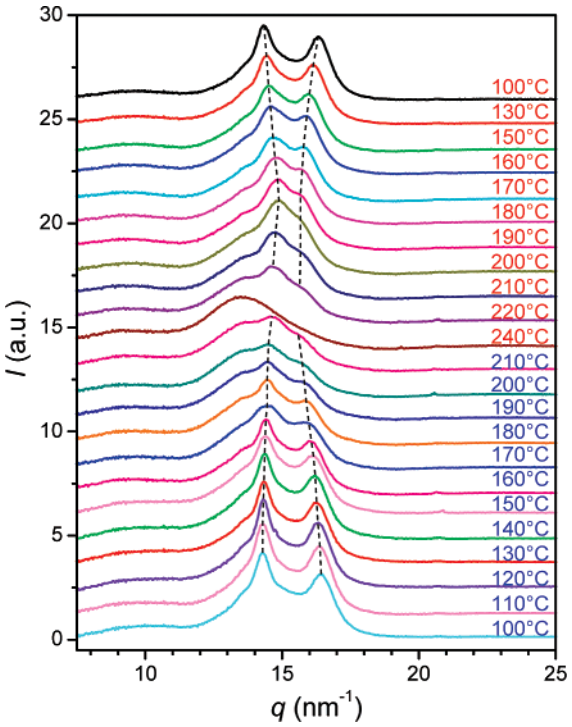

Figure 10. One-dimensional (1D) WAXD profiles for polyimide-confined electrospun nylon-6 nanofibers during stepwise heating (red) and cooling (blue) runs. At each temperature, the sample was isothermally held for 10 min before X-ray detection.

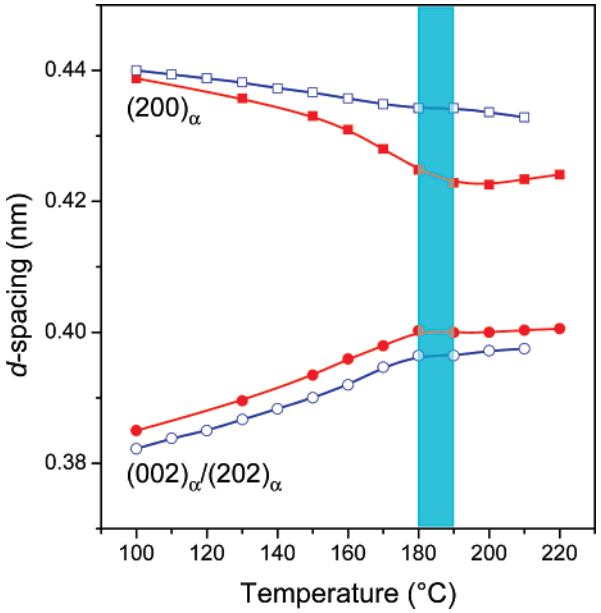

Figure 11. Changes in *d*-spacings of the $(200)_\alpha$ and $(002)_\alpha/(202)_\alpha$ reflections during stepwise heating (red symbols) and cooling (blue symbols) processes. The shaded area indicates the reversible Brill transition in polyimide-confined nylon-6 fibers (ca. 200 nm diameter).

above 180−190 °C and did not merge into a single reflection before crystal melting at 240 °C. This was different from the case of nylon-6,6, where the pseudohexagonal phase existed above 160−170 °C. This high-temperature crystal form, which exhibited two separated reflections, was still considered as a monoclinic phase. It was reported that the Brill transition for nylon-6 actually referred to the crystal-to-crystal transition from the low-temperature α-form to this high-temperature monoclinic form.[1] Upon cooling, a reverse trend was seen; the $(200)_\alpha$ and $(002)_\alpha/(202)_\alpha$ reflections gradually shifted apart from each other. However, the shift of the $(002)_\alpha/(202)_\alpha$ reflections was more substantial than that of the $(200)_\alpha$ reflection.

To determine the Brill transition temperature (T_{Brill}), the *d*-spacing changes as a function of temperature during the heating and cooling cycle in Figure 10 is plotted in Figure 11. Upon heating, *d*-spacings of the $(200)_\alpha$ and $(002)_\alpha/(202)_\alpha$ reflections nearly stopped moving toward each other in a temperature range of 180−190 °C. Therefore, the lower limit of the Brill transition in 200 nm confined nylon-6 fibers can be determined as 180 °C. The *d*-spacing changes during the cooling process also confirmed this conclusion, although there was no substantial change in the *d*-spacing of the $(200)_\alpha$ reflection. Obviously, the T_{Brill} at 180 °C for nanoconfined nylon-6 fibers is at least 20 °C higher than the T_{Brill} at 160 °C for unconfined nylon-6 reported in the literature.[1,47] On the basis of this study, we conclude that the Brill transition of nylon-6 in the electrospun nanofibers with the diameter of 200 nm was "pushed" to a higher temperature of 180 °C, possibly due to the nanoconfinement effect.

Conclusions

Nylon-6 nanofibers with diameters of ~200 nm have been prepared by the electrospinning method. The nanofibers were collected either as a loosely oriented fabric by using a home-built roller or as a highly aligned bundle using a U-shaped metal device. In the as-electrospun nylon-6 nanofibers, the γ-crystalline form was in predominant in the crystals. 1D WAXD results showed that annealing the unconfined nanofibers at elevated temperature (160−180 °C) induced melting of γ-form crystals, followed by recrystallization into α-form crystals. During a DSC heating process, as-electrospun nanofibers exhibited a large exothermic peak before eventual melting of nylon-6 crystals at 220 °C. Because this exothermic peak had twice the heat of transition of that of the melting peak, we conclude that both melt−recrystallization and release of surface tension contributed to this large exothermic peak during heating for as-electrospun nylon-6 nanofibers. PI-coated nylon-6 nanofibers did not show any melt-recrystallization until 210 °C, which was only 10 °C below the T_m. Intriguingly, no exothermic peak was observed for the PI-confined nanofibers before crystal melting.

Crystal orientation was studied by polarized FTIR in as-electrospun nylon-6 nanofibers, where the chain axes (both in the amorphous and γ-form) were oriented parallel to the fiber direction. The γ-crystal orientation was confirmed by a 2D WAXD study. After melting PI-coated nanofibers at 240 °C and recrystallization at 100 °C, α-form crystals were obtained, which had a preferred crystal orientation with the chain axes perpendicular to the fiber direction. The different crystal orientation from that in as-electrospun nanofibers suggested that preferred crystal growth along the *a*-axes of α-form crystals conformed to the fiber axis probably because of a nanoconfinement effect. More intriguingly, the nanoconfinement effect causes the Brill transition to be observed at 180−190 °C for PI-confined nylon-6 nanofibers, which was about 20 °C higher than that in unconfined nylon-6 at ~160 °C. We speculate that nanoconfinement from the high-T_g polyimide effectively restricted volume expansion during both the melt−recrystallization and the Brill transition in nylon-6 nanofibers.

Acknowledgment. H.F. thanks support from the National Institutes of Health/National Institute of Dental and Craniofacial Research (R03 DE16042) and from the US Army Research Laboratory (the Cooperative Agreement No.: DAAD19-02-2-

0011). H.F. also thanks the "Center for Accelerated Applications at the Nanoscale (CAAN)" at the South Dakota School of Mines and Technology (SDSM&T) for support on this project. L.Z. thanks support from the National Science Foundation CAREER Award (DMR-0348724). The synchrotron X-ray experiments were carried out at the National Synchrotron Light Source in Brookhaven National Laboratory, supported by the Department of Energy. Assistance from Dr. Lixia Rong and Prof. Benjamin Hsiao at State University of New York at Stony Brook for the synchrotron X-ray experiments is gratefully acknowledged. The 6FDA−PFMB sample was provided by courtesy of Prof. Frank Harris at the University of Akron.

References and Notes

(1) Murthy, N. S.; Curran, S. A.; Aharoni, S. M.; Minor, H. *Macromolecules* **1991**, *24*, 3215−3220.
(2) Murase, S.; Hirami, M.; Nishio, Y.; Yamamoto, M. *Polymer* **1997**, *38*, 4577−4585.
(3) Murthy, N. S.; Bray, R. G.; Correale, S. T.; Moore, R. A. F. *Polymer* **1995**, *36*, 3863−3873.
(4) Murthy, N. S.; Correale, S. T.; Moore, R. A. F. *J. Appl. Polym. Sci., Appl. Polym. Symp.* **1991**, *47*, 185−197.
(5) Gianchandani, J.; Spruiell, J. E.; Clark, E. S. *J. Appl. Polym. Sci.* **1982**, *27*, 3527−3551.
(6) Arimoto, H.; Ishibashi, M.; Hirai, M.; Chatani, Y. *J. Polym. Sci., Part A: Gen. Pap.* **1965**, *3*, 317−326.
(7) Wunderlich, B. *Macromolecular Physics*; Academic Press: New York, 1973; Vol. 1.
(8) Holmes, D. R.; Bunn, C. W.; Smith, D. J. *J. Polym. Sci., Part A: Gen. Pap.* **1955**, *17*, 159−177.
(9) Li, Y.; Goddard, W. A., III *Macromolecules* **2002**, *35*, 8440−8455.
(10) Ibanes, C.; De Boissieu, M.; David, L.; Seguela, R. *Polymer* **2006**, *47*, 5071−5079.
(11) Park, S.-Y.; Cho, Y.-H.; Vaia, R. A. *Macromolecules* **2005**, *38*, 1729−1735.
(12) Lincoln, D. M.; Vaia, R. A.; Krishnamoorti, R. *Macromolecules* **2004**, *37*, 4554−4561.
(13) Lincoln, D. M.; Vaia, R. A.; Wang, Z. G.; Hsiao, B. S. *Polymer* **2000**, *42*, 1621−1631.
(14) Lincoln, D. M.; Vaia, R. A.; Wang, Z. G.; Hsiao, B. S.; Krishnamoorti, R. *Polymer* **2001**, *42*, 9975−9985.
(15) Murthy, N. S.; Aharoni, S. M.; Szollosi, A. B. *J. Polym. Sci., Polym. Phys. Ed.* **1985**, *23*, 2549−2565.
(16) Aharoni, S. M. *n-Nylons: Their Synthesis, Structure, and Properties*; John Wiley & Sons: New York, 1997.
(17) Formhals, A. U.S. Patent, 1,975,504, 1934.
(18) Baumgarten, P. K. *J. Colloid Interface Sci.* **1971**, *36*, 71−79.
(19) Larrondo, L.; Manley, R. J. *J. Polym. Sci., Polym. Phys. Ed.* **1981**, *19*, 909−919.
(20) Larrondo, L.; Manley, R. J. *J. Polym. Sci., Polym. Phys. Ed.* **1981**, *19*, 921−932.
(21) Larrondo, L.; Manley, R. J. *J. Polym. Sci., Polym. Phys. Ed.* **1981**, *19*, 933−940.
(22) Cheng, J. Y.; Ross, C. A.; Smith, H. I.; Thomas, E. L. *Adv. Mater.* **2006**, *18*, 2505−2521.
(23) Doshi, J.; Reneker, D. H. *J. Electrostatics* **1995**, *35*, 151−160.
(24) Reneker, D. H.; Chun, I. *Nanotechnology* **1996**, *7*, 216−223.
(25) Fong, H.; Reneker, D. H. Electrospinning and Formation of Nanofibers. In Salem, D. R., Ed.; *Structure Formation in Polymeric Fibers*; Hanser Gardner: Cincinnati, 2001; pp 225−246.
(26) Jaeger, R.; Bergshoef, M. M.; Batlle, C. M. I.; Schonherr, H.; Vancso, G. J. *Macromol. Symp.* **1998**, *127*, 141−150.
(27) Bognitzki, M.; Czado, W.; Frese, T.; Schaper, A.; Hellwig, M.; Steinhart, M.; Greiner, A.; Wendorff, J. H. *Adv. Mater.* **2001**, *13*, 70−72.
(28) Deitzel, J. M.; Kleinmeyer, J.; Harris, D.; Tan, N. C. B. *Polymer* **2001**, *42*, 261−272.
(29) Deitzel, J. M.; Kleinmeyer, J. D.; Hirvonen, J. K.; Tan, N. C. B. *Polymer* **2001**, *42*, 8163−8170.
(30) Kalayci, V. E.; Patra, P. K.; Buer, A.; Ugbolue, S. C.; Kim, Y. K.; Warner, S. B. *J. Adv. Mater.* **2004**, *36*, 43−47.
(31) Reneker, D. H.; Yarin, A. L.; Fong, H.; Koombhongse, S. *J. Appl. Phys.* **2000**, *87*, 4531−4547.
(32) Yarin, A. L.; Koombhongse, S.; Reneker, D. H. *J. Appl. Phys.* **2001**, *89*, 3018−3026.
(33) Shin, Y. M.; Hohman, M. M.; Brenner, M. P.; Rutledge, G. C. *Appl. Phys. Lett.* **2001**, *78*, 1149−1151.
(34) Kotek, R.; Jung, D.; Tonelli, A. E.; Vasanthan, N. *J. Macromol. Sci., Polym. Rev.* **2005**, *C45*, 201−230.
(35) Bellan, L. M.; Kameoka, J.; Craighead, H. G. *Nanotechnology* **2005**, *16*, 1095−1099.
(36) Dersch, R.; Liu, T.; Schaper, A. K.; Greiner, A.; Wendorff, J. H. *J. Polym. Sci., Part A: Polym. Chem.* **2003**, *41*, 545−553.
(37) Stephens, J. S.; Chase, D. B.; Rabolt, J. F. *Macromolecules* **2004**, *37*, 877−881.
(38) Liu, Y.; Pellerin, C. *Macromolecules* **2006**, *39*, 8886−8888.
(39) Bergshoef, M. M.; Vancso, G. J. *Adv. Mater.* **1999**, *11*, 1362−1365.
(40) Fong, H.; Liu, W. D.; Wang, C. S.; Vaia, R. A. *Polymer* **2002**, *43*, 775−780.
(41) Murase, S.; Kashima, M.; Kudo, K.; Hirami, M. *Macromol. Chem. Phys.* **1997**, *198*, 561−572.
(42) Li, F.; Kim, K.; Kulig, J.; Savitski, E.; Brittain, W.; Harris, F.; Cheng, S.; Hubbard, S.; Singer, K. *J. Mater. Chem.* **1995**, *5*, 253−259.
(43) Zhu, L.; Calhoun, B. H.; Ge, Q.; Quirk, R. P.; Cheng, S. Z. D.; Thomas, E. L.; Hsiao, B. S.; Yeh, F.; Liu, L.; Lotz, B. *Macromolecules* **2001**, *34*, 1244−1251.
(44) Fornes, T. D.; Paul, D. R. *Polymer* **2003**, *44*, 3945−3961.
(45) Wunderlich, B. *Thermal Analysis*; Academic Press: Boston, 1990; p 206.
(46) Tashiro, K.; Takeuchi, K.; Ohta, Y.; Hanesaka, M.; Hashida, T.; Yoshioka, Y.; Ramesh, C. *Macromol. Symp.* **2006**, *242*, 250−256.
(47) Vasanthan, N.; Murthy, N. S.; Bray, R. G. *Macromolecules* **1998**, *31*, 8433−8435.

MA070039P